Assessing the operating temperature of multi-junction solar cells with novel rear side layer stack and local electrical contacts

D. Alonso-Álvarez[1,], C. Weiss[2], J. Fernandez[2,†], S. Janz[2] and N. Ekins-Daukes[1,3]*

[1] Department of Physics, Imperial College London, London, SW7 2AZ, United Kingdom

[2] Fraunhofer Institute for Solar Energy Systems, Freiburg, 79110, Germany

[3] School of Photovoltaic & Renewable Energy Engineering, UNSW Sydney, Kensington NSW 2052, Australia

Abstract:

Sub-bandgap sunlight provides a source of heat generation in solar cells that is detrimental to performance, especially in space applications where heat dissipation is limited. In this work we assess the impact that an advanced rear-side contact scheme for multi-junction solar cells has on the cell temperature. Our results show that this scheme reduces the optical power absorption below the bandgap of germanium by 81% compared to a standard, full metallization design. Measurements of the electrical and thermal power fluxes performed in vacuum demonstrate that this lower near-infrared light absorption results in 8% less heat dissipated in the cell with the novel rear-side contact scheme when operating at 25 ºC. Modelling of the operating temperature for both cells when fully encapsulated with glass indicates that this effect will also result in a reduction of the operating temperature of 9 ºC for the novel design.

Keywords: multi-junction solar cells; temperature; space photovoltaics; germanium; characterisation

[*] Corresponding author: d.alonso-alvarez@imperial.ac.uk

[†] Now with: Total, La Défense Cedex, 92078, Paris, France

1. Introduction

The operating temperature has a major impact on the performance of solar cells, both for terrestrial applications and in space [1]. In the former, several channels exist to dissipate the waste heat from the module, from simple natural convection in traditional planar solar panels [2], to sophisticated heat-sinks in concentrator photovoltaic systems for passive cooling [3], [4], or active cooling with fluid circulation [5], [6]. In solar cells used for space applications, the only way of removing the waste heat is through thermal radiation, which requires a careful optimization of the thermal and optical properties of the materials. While the dependence of the solar cell performance with temperature is well understood [7] and there are simple approximate methods to calculate the operating temperature of space solar cells [8], the role sub-gap infrared (IR) light absorption has generally not been considered.

In a recent work, a new design of MJ solar cell with a back mirror and point electrical contacts has shown superior Ge bottom cell performance [9]. This design was also predicted to reduce the operating temperature of the cell by reflecting the unused near infrared solar photons [9], [10]. In this work we demonstrate that this novel design does indeed result in a lower operating temperature. We characterise the electrical and thermal properties of the device under vacuum conditions and compare the results against numerical radiation balance models that use the measured absorptivity and emissivity as inputs.

2. Materials and methods

2.1. Samples description

Two metamorphic triple junction solar cells were processed on p-doped Ge substrate, called the standard sample and the laser-fired contact (LFC) sample, depicted in Fig. 1a and 1b. In both cells, the III-V layers ($Ga_xIn_{1-x}As$ with a bandgap of 1.18 eV and $Ga_yIn_{1-y}P$ with a bandgap of 1.74eV) are grown on Ge substrates, have metal fingers on the front side and an anti-reflection coating (ARC). The details on the metamorphic growth process are described in Ref. [10]. The metamorphic growth ensures that the currents from all three sub-cells under air-mass 0 spectrum are nearly equal, improving upon the conventional lattice-matched structure where photogenerated current in the Ge cell is wasted. The standard sample (Fig. 1a) is grown on Ge-substrate with a doping level of 2×10^{17} cm^{-3}, whereas the LFC sample (Fig. 1b) is grown on a low doped Ge-substrate of 2×10^{16} cm^{-3}. The backside of the standard sample consists of aluminium (Al) directly evaporated on Ge. The LFC sample back side consists of an a-Si_xC_{1-x} passivation layer, followed by a SiO_2 mirror layer and evaporated Al on top. After the metallization, the LFC sample is contacted via a laser process, which drives the Al through the a-Si_xC_{1-x} /SiO_2 layer stack into the Ge substrate, leading to the formation of point contacts and to a local back surface field (p^{++} LBSF) under the point contacts, due to local Al doping of the Ge. The point contacts have a diameter of 100 µm and a periodicity of 300 µm. This

results in about 9% of the LFC sample's rear side opened by the laser process. For comparison, a third cell (Fig. 1c) with low (1×10^{16} cm^{-3}) doping in the Ge wafer and a rear full metallization based on Ti/Pd/Ag has also been studied. The Ti/Pd/Ag metallization provides a good electrical contact, but a low reflectivity. Therefore, the cell is called "No mirror" cell. It was produced and measured to separate the role of the doping of the Ge wafer and the rear mirror on the absorptivity of the triple junction cell

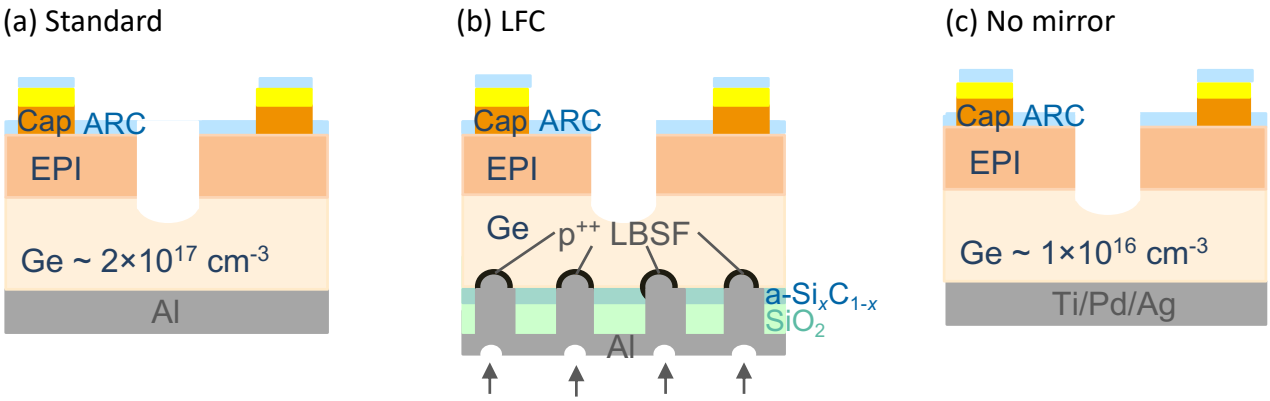

Figure 1: Diagram of the structure of the solar cells used in this work. (a) Standard cell with high Ge doping, (b) LFC cell with low Ge doping and (c) cell with low Ge doping and no rear side mirror.

2.2. Electrical and optical characterization

The near (NIR) and mid-infrared (MIR) absorptivity (=emissivity) of the solar cells were measured using a Bruker Vertex 70 FTIR system equipped with a gold-coated integrating sphere and a liquid nitrogen-cooled HgCdTe detector by Infrared Associates Inc. Band edge reflectivity measurements of the no mirror cell have been done with a PerkinElmer Lambda900 spectrometer. Measurements of the short circuit current and the open circuit voltages were done with a Keithley 2000 multimeter. The maximum power point tracking was performed using a Keithley 2620 source meter unit using a 4-wire configuration. The initial current voltage (IV) characterization of the cells was performed using a one-zone solar simulator under AM1.5 global spectrum (1000 W/m², uncalibrated) at 25°C.

2.3. Thermal characterization

In order to characterise the effect of the different solar cell designs on the operating temperature, a special temperature-controlled stage was built within a vacuum chamber in order to supress convective heat losses, to mimic conditions in space. Figure 2 shows a schematic diagram of this system with its components. The sample was attached to a copper block with thermally and electrically conductive silver paste (Figure 2a). This block served as back contact for the electrical measurements whereas the front contact of the cell was made using thin needle probes installed inside the chamber. A thermocouple embedded in the copper block monitored the sample temperature. The block was fixed with thermally conductive silicone to a heat flux sensor (Omega

HFS-4) and this to the hot side of a Peltier cooler. The cold side of the cooler was attached to a larger copper plate in thermal contact to the structure of the chamber. The vacuum chamber had a quartz window (Figure 2b), with high transparency in the NIR and opaque in the MIR. The illumination was provided by a one-zone solar simulator with a xenon bulb, around 1363 W/m^2 of total power and a spectrum similar to the air-mass 0 spectrum (uncalibrated). Typical pressure inside the chamber during the experiments was ≤ 10^{-4} mbar. Fans outside the chamber kept the temperature of the walls and the window roughly at room temperature. This temperature was controlled by an air conditioning system in the room and set to 25 ºC. All temperatures, as well as the signal from the flux sensor, were recorded with a Pico TC-08 data logger.

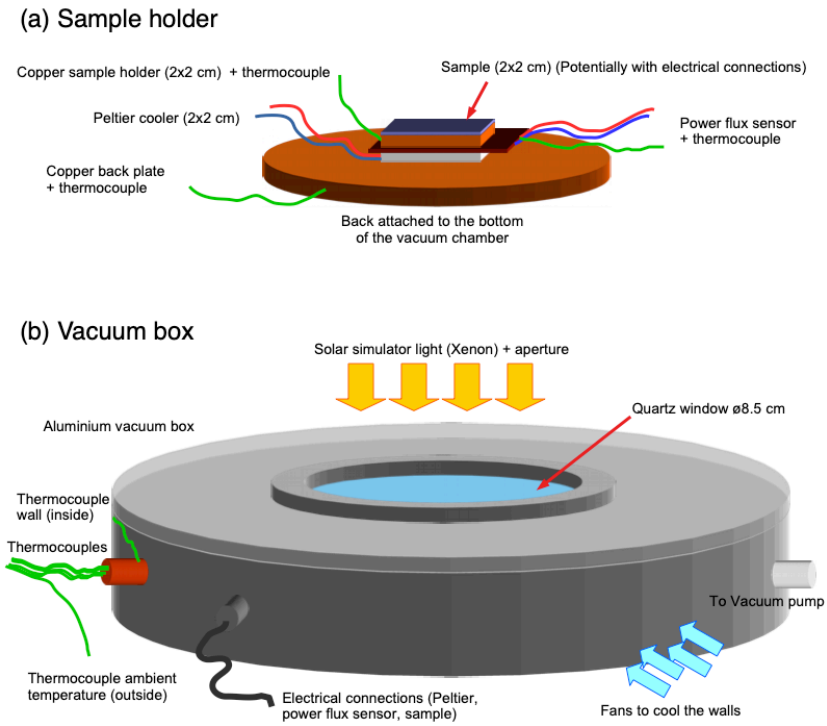

Figure 2: (a) Diagram of the sample holder and the heat extraction setup. (b) General diagram of the vacuum box.

3. Theory

Under illumination, the optical power absorbed by the solar cell (P_{Sun}) will follow different routes. To a first approximation the energy flows are [11]:

1) extracted as electrical power (P_{el}),
2) re-emitted as thermal radiation through the front surface (P_{front}), and
3) extracted from the back (P_{back}).

In a real application, as part of a solar panel for space, the heat extraction through the back of the solar collector will also occur by the emission of thermal radiation to the outer space and will depend on the cell temperature. In this work, this is forced through the heat flux sensor by applying a current

to the Peltier cooler. Including the influence of thermal radiation from the walls of the vacuum chamber (P_A) kept at ambient temperature $T_A = 25\,ºC$, the balance of power will be:

$$P_{Sun} + P_A(T_A) = P_{el}(T_{cell}) + P_{front}(T_{cell}) + P_{back} \quad (1)$$

P_{Sun} depends on the absorptivity of the cell in the visible and NIR ranges while P_A and P_{front} depend on the MIR absorptivity. As P_{back} is changed, a new equilibrium cell temperature will be reached dependent on its emissivity and the dependence of the electrical power with temperature, usually following a linear relationship:

$$P_{el}(T_{cell}) = P_{25}[1 + \beta(T_{cell} - T_{25})] \quad (2)$$

with $T_{25} = 25\,ºC$, P_{25} the power at T_{25} and β the thermal coefficient, which is negative indicating lower power at higher operating temperatures. Further details on the relationship of the terms in Eq. 1 with the temperature and the emissivity can be found in [11].

4. Results

4.1. Electrical characterization

The IV characteristics of the standard sample (doping 2×10^{17} cm^{-3}, Al back contact) and the LFC sample (doping 2×10^{16} cm^{-3}, passivation + LFC contact) before the thermal experiments are depicted in Figure 3. The LFC sample shows a slightly higher I_{SC} than the standard sample, whereas for the latter, a higher V_{OC} is measured. The increase in I_{SC} for the LFC sample is the expected benefit from a successful Ge back side passivation and reduced parasitic free carrier absorption. Such increase in I_{SC} is only to be expected in solar cells where the Ge junction is not overproducing current, as it is the case in metamorphic designs. In principle, a lower V_{OC} is also expected for lower doped Ge substrate and therefore for the LFC sample. However, simulations have shown that an optimized passivation can compensate the loss in V_{OC} due to a lower doping level [9]. Therefore, the difference in V_{OC} and I_{SC} between the standard and the LFC sample in Figure 3 are attributed to a good, but sub-optimal back side passivation.

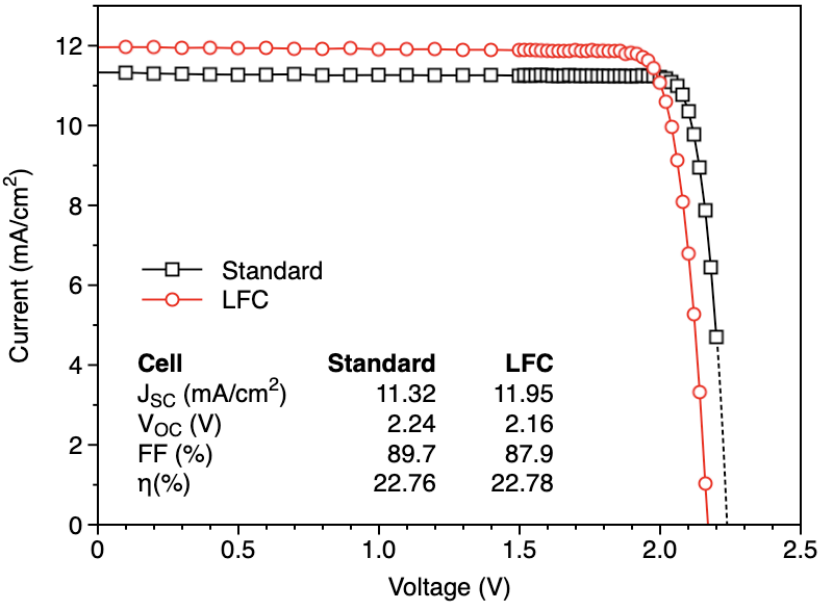

Figure 3: IV curves of the two solar cells before any thermal cycles. Dashed line in the standard cell curve is extrapolated data.

4.2. Emissivity

Figure 4a shows the thermal emissivity of the two solar cells together with the AM0 solar spectrum. Up to the germanium bandgap (vertical dashed line) both cells are roughly the same. At longer wavelengths, though, the standard cell has higher emissivity than the LFC cell due to the free carrier absorption in the highly doped germanium. This has two consequences: 1) the standard sample will absorb more sub-gap NIR sunlight that serves only to increase the cell temperature and 2) it will emit more MIR radiation. The reduction in NIR power absorption can be calculated as:

$$\Delta P = \frac{\int_{\lambda_{Ge}}^{\infty} \left(Abs_{Standard}(\lambda) - Abs_{LFC}(\lambda)\right) \times AM0(\lambda) d\lambda}{\int_{\lambda_{Ge}}^{\infty} Abs_{Standard}(\lambda) \times AM0(\lambda) d\lambda} \times 100$$

This calculation indicates that the LFC cell will absorb 81% less NIR solar power than the standard cell based on the measured absorptivity.

Figure 4b shows the emissivity (=absorptivity) of the same cells in comparison to the cell with low Ge doping & no rear mirror. The absorptivity of the later is similar to that of the standard cell, indicating that the extraordinary reduction of the absorptivity in the LFC cell is not only due to the lower doping in the Ge wafer, but indeed consequence of the SiO_x mirror and point contacts, which restricts the area of heavy doping in the back of the cell. This finding for the Ge sub-cell agrees with observations from silicon solar cells, where a large fraction of the NIR and MIR emissivity comes from the heavily doped back surface field layer resulting from the annealing of the continuous metal contact [14]. This result is one of the expected consequences of the novel rear stack, similar to the

findings of Fernandez *et al.*, and it should result in lower operating temperature for the LFC cell assuming the same power extraction [10].

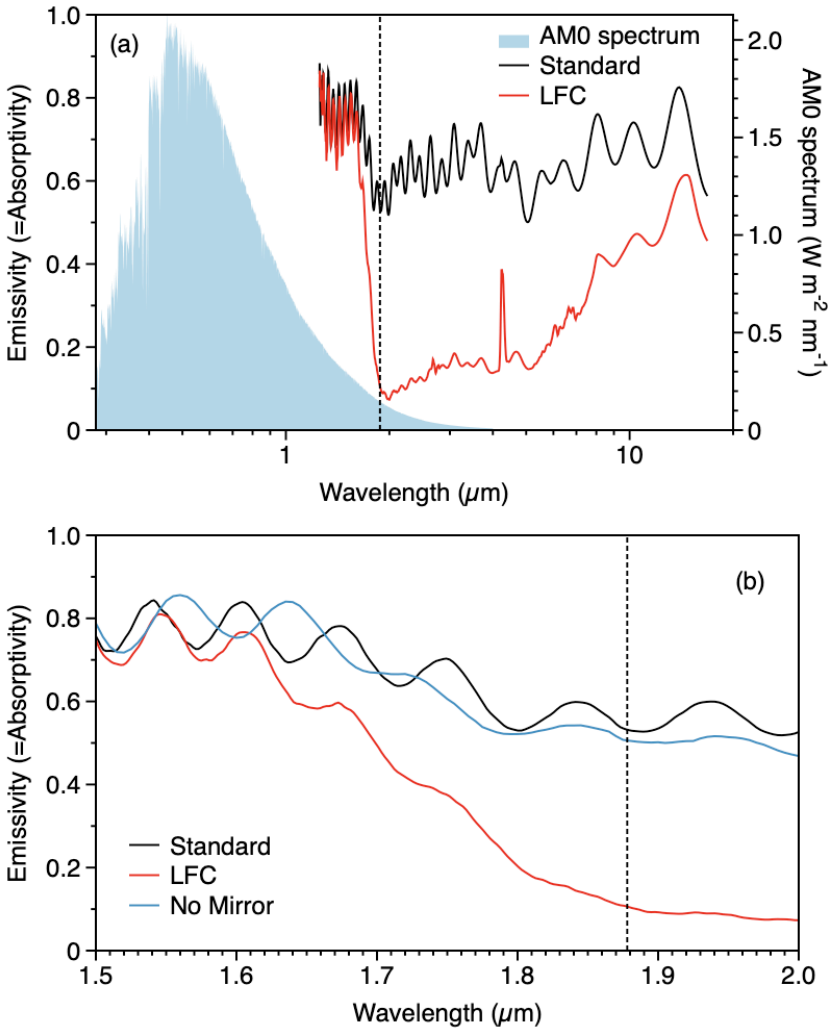

Figure 4: (a) NIR and MIR emissivity of the standard and LFC solar cells together with the AM0 solar spectrum. (b) Detail of the near band edge reflectivity of the standard, LFC and no mirror cells.

4.3. Thermal cycles

As it is described earlier (Section 3), changing the power extracted through the back of the cell, P_{back}, will force the sample to reach a new equilibrium temperature where the power absorbed is balanced by the total power extracted from the cell by any means. Two cells with identical electrical properties but different NIR and MIR emissivities will reach a different equilibrium temperature for the same P_{back} as P_{front} and P_{Sun} will differ, in general.

Figure 5 shows a typical thermal cycle with the cell in open circuit and therefore without extraction of electrical power ($P_{el} = 0\ W/m^2$). The temperature of the sample, T_{Cell}, increases as the thermal flux through the sensor attached to the back, P_{back}, decreases. This flux is controlled by the Peltier module. When no thermal flux is allowed to flow towards the back ($P_{back} = 0\ W/m^2$), the sample has to dissipate all the heat radiatively, via P_{front}, which is a less efficient process, and therefore its

temperature increases. Each time that the current applied to the Peltier changes, it is necessary to wait around 15-20 minutes for the temperature and the power flux to become stable again. Once they become stable, pairing the temperature of the sample with each power flux it is possible to draw some conclusions on the thermal performance of the cell and the role of the rear stack. This thermal cycle can be done under different electrical conditions, with the cell at short circuit (SC), open circuit (OC) and kept at maximum power point (MPP).

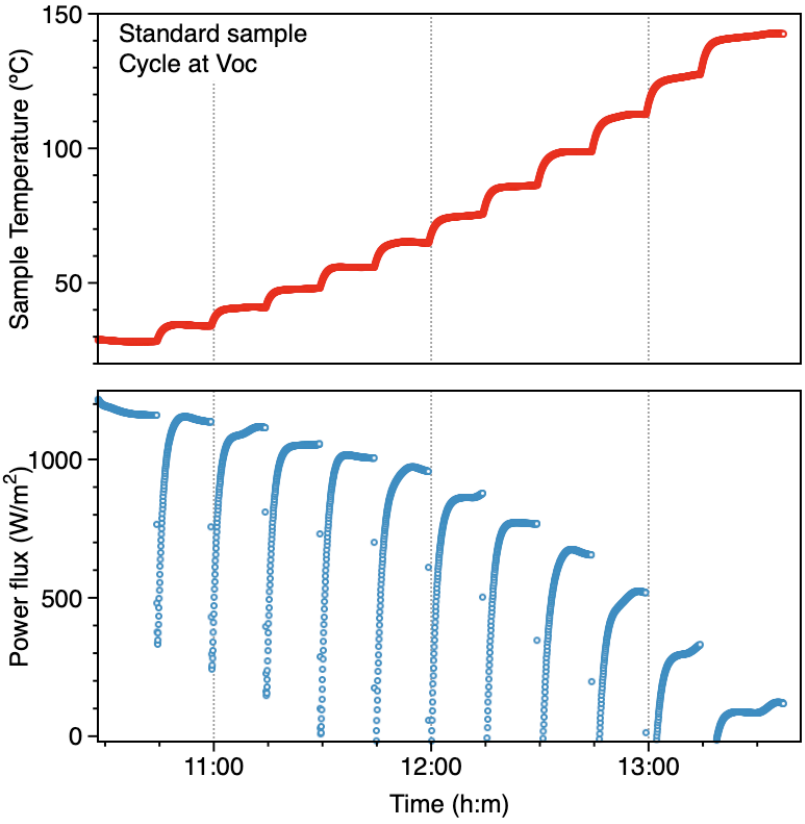

Figure 5: Example of thermal cycle, showing the sample temperature (top) and the power flux through the sensor (bottom).

Figure 6 shows the T_{cell} vs P_{back} curves for the two samples under the three electrical conditions: SC, OC and MPP. For the MPP case, P_{el} and $P_{el} + P_{back}$ are also shown. First, we consider the comparison between the P_{back} curves measured at SC, OC and MPP conditions. For both cells, the curve at OC is above that of SC, and both are above the one at MPP. It is expected for the later to be the lowest since at MPP a significant amount of the incoming power (around 22%) is extracted electrically [12]. This electrical power P_{el} decreases linearly with temperature with a coefficient β of -0.27%/K and -0.25%/K for the standard and LFC cells, respectively, in agreement with reported results for the MJ solar cell architecture [13]. Having the curves at SC below those at OC suggest the presence of some resistive power loss in the external circuit, leaving less available to be extracted through the thermal flux sensor. A final interesting result is that the addition of the electrical

and thermal powers at MPP $P_{el} + P_{back}$ is higher than any of the other two, in particular at low temperatures. This result suggests that some parasitic losses, present in the other cases, are suppressed when part of the power is electrically extracted; these parasitic losses are discussed further in Section 5.3.

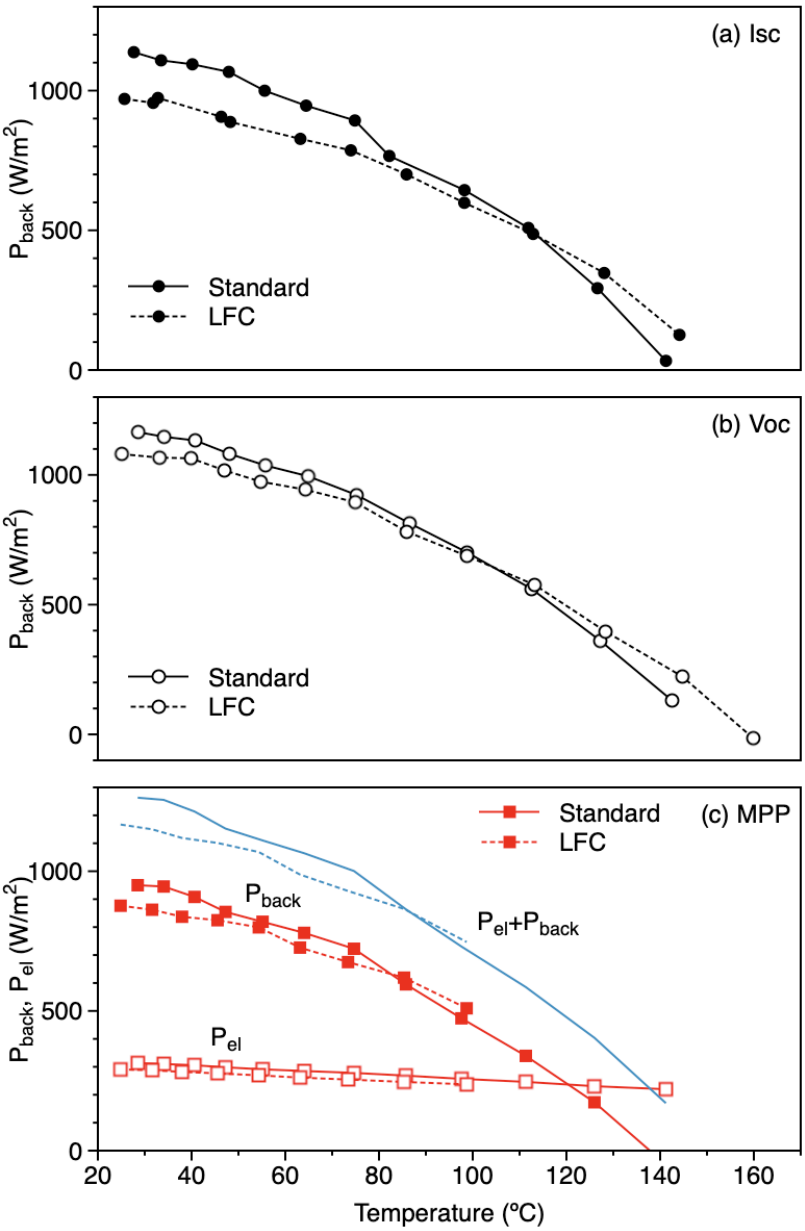

Figure 6: P_{back} vs temperature curves for the standard and the LFC solar cell at (a) short circuit and (b) open circuit. (c) P_{back} and P_{el} at maximum power point.

The power that needs to be extracted at room temperature depends only on the amount of sunlight absorbed and the electrical power extracted since $P_{front} = P_a$ in this case. If one sample is compared with the other, we can see that this power is higher for the standard cell than for the LFC cell, as anticipated based on the emissivity measurements shown in Figure 4. Looking at the MPP curves (Figure 6c), it can be seen that in order to keep the cells at 25 ºC, it is necessary to extract 948 W/m^2 for the standard cell and 872 W/m^2 for the LFC cell. This is a reduction of 8%, consequence of the

lower NIR absorptivity of the LFC cell. As less power is extracted, the higher absorption of sunlight by the standard cell is compensated by its also higher thermal emission. As a consequence, from about 85 ºC, the curves of the LFC cell are above those of the standard cell. The LFC cell failed during the MPP cycle (the last one to be done) and there is no reliable data beyond 100 ºC, but the SC and OC curves suggest that for a zero extracted power, its temperature would be around 10-15 ºC higher than for the standard cell.

The crossover between the curves of both cells also points to an interesting result: for an operating temperature of 85 ºC, both designs will require the same amount of thermal power to be extracted, regardless of the design of the rear side. This statement, however, needs to be taken with caution since the cover glass – present in reality in any solar module – has high MIR emissivity. In Section 5.2 the effect that the cover glass will have in the solar cell temperature is estimated.

5. Discussion

5.1. Modelling the solar cell temperature

Based on the measured emissivity of the cells, we can model the power vs temperature curves in the ideal case and, by comparison with the experimental result, extract some information on the parasitic losses. In this section, we assume that the absorptivity of both cells above the bandgap of Ge is the same and equal to 0.9, for simplicity. For the NIR and MIR, the measured values shown in Figure 4 are used.

Figure 7 shows the calculated curves for the two samples at MPP, using the linear relationship found in Section 4.3 for P_{el}. The mathematical details were outlined in Section 3 and described in more detail in Alonso-Álvarez *et al*. [11]. The continuous curves are the equilibrium temperatures resulted from Eq. 1 using P_{back} as the free variable. It can be seen that they qualitatively reproduce the experimental behaviour, showing a reduction of the extracted power at 25 ºC of around 6% between the standard and the LFC samples. However, these curves extend toward higher temperatures, with zero extracted power temperatures of 155 ºC and 213 ºC, for the standard and LFC samples, respectively. This is significantly higher than the 134 ºC and 145 ºC (estimated) values obtained experimentally. In Section 5.3 this discrepancy is explained by several parasitic losses present in the experiment and not accounted for in the model.

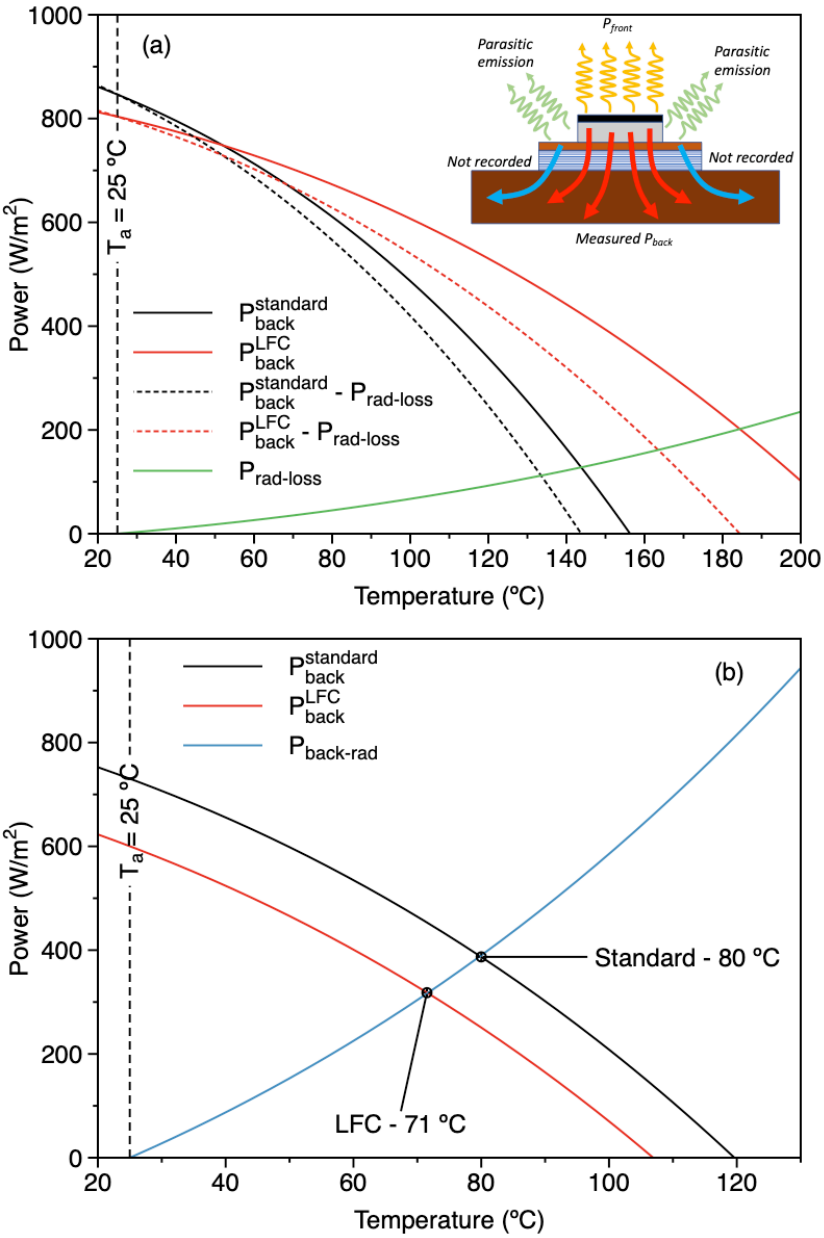

Figure 7: (a) Modelled power vs temperature curves for the standard and the LFC solar cells in the ideal case (continuous lines) and considering radiative parasitic losses (dashed lines). (b) Modelled power vs temperature curves in the ideal case when the emissivity of the front surface is 0.9, corresponding to a glass cover, as well as the thermal radiation of the back surface assuming an emissivity of 0.9.

5.2. Effect of cover glass and radiative emission from the back

Solar cells used in space are always encapsulated with high emissivity glass that promotes radiative heat dissipation. This coverglass has typical emissivity values in the range of 0.85-0.95 and dominates the thermal emission of the cell. We can repeat the ideal calculations of Figure 7a using an emissivity of 0.9 rather than the emissivity of the underlaying cells to obtain P_{front} and P_a. The result of this calculation is shown in Figure 7b. Two effects can be observed: first, the maximum

temperature of the cells and the extracted power are much lower than before due to the higher thermal radiation through the front surface; and second, the temperature of the LFC cell is always below that of the standard cell, rather than crossing at a certain point, thanks to the lower absorption of NIR photons of the LFC design.

Finally, as it has been pointed out, in a space array, heat through the back of the cell is ultimately dissipated radiatively into outer space. The blue line in Figure 7b shows the calculated power radiated through the back as a function of the cell temperature assuming the rear of the space array has an emissivity of 0.9. The equilibrium temperatures that the cells would reach if this were the mechanism for dissipating heat through the back are 80 ºC and 71 ºC for the standard and LFC cells, respectively. Therefore, a decrease of 9 ºC in the solar cell operating temperature due to the use of the novel back contact design should be possible. It should be noted that an ambient temperature of $T_a = 25\,ºC$ has been used in all these calculations. In space, however, the temperature to use could be significantly lower – as low as 3 K, which is the background cosmic temperature – and will depend on the exact location of the solar cells, distance to the Earth surface (or other planets) and their orientation. In Fernandez *et al.* temperatures of 52 ºC and 45 ºC are reported for solar cells with back-side technologies similar to those of this work in a geostationary orbit, although no details are provided of such calculations [10].

5.3. Parasitic losses

There are three main sources of parasitic losses in the measurements that are not accounted for in the simulations. The first is thermal emission from the sample holder and the front of the flux sensor, P_{rad_loss}. While both were covered with low emissivity aluminium tape, their area is significant (around 2.5 times that of the solar cell) and therefore the heat dissipated from those surfaces cannot be disregarded. The green continuous curve in Figure 7a shows an estimate of that parasitic loss, calculated using the emissivity of aluminium (measured as 0.08 at 8 μm). While it is small at low temperature, it becomes significant at higher temperatures and it results in the dashed curves when it is considered in the overall calculations.

The second parasitic loss is related with the limited active area of the flux sensor (2×2 cm^2, equal to the area of the sample holder) compared with its total area (3.5×2.8 cm^2). This discrepancy means that part of the power extracted from the back with the Peltier cooler is not being recorded by the sensitive area of the flux sensor. This parasitic conduction loss, P_{cond_loss}, is difficult to quantify but, should be small considering that vertical heat transport across the thin flux sensor should be much faster than in-plane transport away from the sensitive area.

The final parasitic loss is related with conductive thermal transport along the cables connected to the sample (including the electrical cables and the thermocouples), P_{cable_loss}. Those cables can conduct heat away from the sample, especially at high temperature. While this loss is not considered

in the model, it is an unavoidable heat dissipation process that will be also present in real working conditions as part of the electrical interconnections of the solar panel.

Addressing the differences between the curves taken at SC, OC and MPP requires a more detailed electro-thermal modelling similar to the one described in Couderc *et al.* for silicon solar cells [12]. Adapting such a model for MJ devices is outside the scope of this paper, though. This model should consider all power fluxes entering and leaving the cell at any temperature, as well as the internal recombination mechanisms, also as a function of the voltage.

5.4. Real solar cell temperature

In the discussion of the experimental results, it has been assumed that the temperature measured with the thermocouple of the copper block the solar cell is attached to is the real solar cell temperature. However, it is expected that the real solar cell temperature to be higher due to the thermal resistance arising from the thermal adhesive between the copper and the cell, and also the insulating layers in the rear of the LFC solar cell. This difference is difficult to quantify, but the effect will be larger at higher measured temperatures. Considering the experimental curves of Figure 6, if this effect is included, the results will be qualitatively closer to the modelled data of Figure 7.

6. Conclusions

In this work, we have presented a thermal and electrical analysis of two multi-junction solar cells with different designs: one following a standard architecture and the other with a novel rear contact design that both increases the minority carrier lifetime Ge subcell and reduces the absorption of sunlight below the Ge bandgap (LFC). The results presented here demonstrate that the LFC solar cell has a significantly lower sub-bandgap absorption in the NIR region (81% lower) than the standard design. Moreover, the thermal cycles performed in vacuum show that the LFC sample requires 8% less thermal power to be extracted in order to operate at 25 ºC, a direct consequence of the lower NIR absorptivity. At higher temperatures (>85 ºC), this trend reverses, the standard sample requiring less active thermal power extraction on account of its higher MIR emissivity and therefore higher rate of radiative heat dissipation. With a cover glass and radiative thermal emission through the back, both with thermal emissivity of 0.9, the model predicts that the LFC cell will operate at 71 ºC, 9 ºC lower than the standard cell, which will have a positive impact into the overall electrical performance of the cell.

The modelling of the results agrees qualitatively with the experiments. However, several parasitic mechanisms for heat loss have been identified, that frustrate quantitative modelling of the results. In particular, a rigorous explanation of the differences observed between the measurements at short circuit, open circuit and tracking the maximum power point, will require coupled electro-thermal calculations considering the recombination mechanisms present inside the solar cell as a function of the voltage.

Acknowledgements

This work was funded by the United Kingdom's Engineering and Physical Science Research Council (EPSRC) grants High Temperature, High Efficiency PV-Thermal Solar System (EP/M025012/1), and the Joint UK-India Clean Energy Centre (JUICE) (EP/P003605/1). D. Alonso-Álvarez also wants to thank I. Guarracino, A. Mellor and S. Cussell for the original design and fabrication of the vacuum box setup, as well as Y. Li for its testing during her master thesis.

References

[1] P. Singh and N. M. Ravindra, "Temperature dependence of solar cell performance—an analysis," *Solar Energy Materials and Solar Cells*, vol. 101, no. C, pp. 36–45, Jun. 2012.

[2] M. Mattei, G. Notton, C. Cristofari, M. Muselli, and P. Poggi, "Calculation of the polycrystalline PV module temperature using a simple method of energy balance," *Renewable Energy*, vol. 31, no. 4, pp. 553–567, Apr. 2006.

[3] L. Micheli, E. F. Fernández, F. Almonacid, T. K. Mallick, and G. P. Smestad, "Performance, limits and economic perspectives for passive cooling of High Concentrator Photovoltaics," *Solar Energy Materials and Solar Cells*, vol. 153, no. c, pp. 164–178, Aug. 2016.

[4] I. A. Siyabi, K. Shanks, T. Mallick, and S. Sundaram, "Thermal analysis of a multi-layer microchannel heat sink for cooling concentrator photovoltaic (CPV) cells," presented at the AIP Conference Proceedings, 2017, vol. 1881, no. 1, pp. 070001–9.

[5] I. Guarracino, A. Mellor, N. J. Ekins-Daukes, and C. N. Markides, "Dynamic coupled thermal-and-electrical modelling of sheet-and-tube hybrid photovoltaic/thermal (PVT) collectors," *Applied Thermal Engineering*, vol. 101, no. C, pp. 778–795, May 2016.

[6] N. Gakkhar, M. S. Soni, and S. Jakhar, "Analysis of Water Cooling of CPV Cells Mounted on Absorber Tube of a Parabolic Trough Collector," *Energy Procedia*, vol. 90, pp. 78–88, Dec. 2016.

[7] G. Landis, "Review of solar cell temperature coefficients for space," presented at the Proceedings of the XIII Space Photovoltaic Research and Technology Conference SPRAT XIII, 1994, p. 385.

[8] G. A. Landis, P. Jenkins, D. Scheiman, and R. Rafaelle, "Extended temperature solar cell technology development," presented at the Collection of Technical Papers - 2nd International Energy Conversion Engineering Conference, 2004, vol. 1, pp. 485–491.

[9] C. Weiss, J. Schön, O. Höhn, C. Mohr, R. Kurstjens, B. Boizot, and S. Janz, "Potential Analysis of a Rear-Side Passivation for Multi-Junction Space Solar Cells based on

Germanium Substrates," presented at the IEEE Photovoltaics Specialist Conference, 2018, pp. 1–5.

[10] J. Fernandez, S. Janz, D. Suwito, E. Oliva, and F. Dimroth, "Advanced concepts for high-efficiency germanium photovoltaic cells," presented at the Conference Record of the IEEE Photovoltaic Specialists Conference, 2008, pp. 1–4.

[11] D. Alonso-Álvarez, L. Ferre Llin, A. Mellor, D. J. Paul, and N. J. Ekins-Daukes, "ITO and AZO films for low emissivity coatings in hybrid photovoltaic-thermal applications," *Solar Energy*, vol. 155, pp. 82–92, Oct. 2017.

[12] R. Couderc, M. Amara, and M. Lemiti, "In-Depth Analysis of Heat Generation in Silicon Solar Cells," *IEEE J. Photovoltaics*, vol. 6, no. 5, pp. 1123–1131, Aug. 2016.

[13] E. F. Fernández, G. Siefer, M. Schachtner, A. J. García Loureiro, and P. Pérez-Higueras, "Temperature coefficients of monolithic III-V triple-junction solar cells under different spectra and irradiance levels," presented at the AIP Conference Proceedings, 2012, vol. 1477, no. 1, pp. 189–193.

[14] A. Riverola, A. Mellor, D. Alonso-Álvarez, L. F. Llin, I. Guarracino, C. N. Markides, D. J. Paul, D. Chemisana, and N. Ekins-Daukes, "Mid-infrared emissivity of crystalline silicon solar cells," *Solar Energy Materials and Solar Cells*, vol. 174, pp. 607–615, Oct. 2017.